Electronic intertube transfer in double-wall carbon nanotubes

Seiji Uryu* and Tsuneya Ando
Department of Physics, Tokyo Institute of Technology, 2-12-1 Ookayama, Meguro-ku, Tokyo 152-8551, Japan
(Received 6 June 2005; revised manuscript received 12 September 2005; published 5 December 2005)

Effects of intertube interactions on transport are studied numerically in incommensurate double-wall carbon nanotubes. The intertube transfer at each lattice site oscillates around zero in a complex plane as a function of position in a quasiperiodic manner and therefore cancels each other when being summed up. The cancellation is not perfect in the presence of sharp edges, giving rise to an intertube conductance much smaller than $e^2/\pi\hbar$ and determined by the structure at edges. The conductance exhibits a wild and almost irregular oscillation as a function of the length with average and fluctuations independent of the length due to the change of the edge structure.

DOI: 10.1103/PhysRevB.72.245403 PACS number(s): 73.63.Fg, 73.23.Ad, 72.80.Rj

I. INTRODUCTION

Carbon nanotubes[1] are often self-assembled to be multiwall tubes and bundles. In these systems electrons can transfer from one tube to another and such intertube transfer may modulate electronic properties of constituent single-wall nanotubes. The purpose of this paper is to clarify intertube effects on their transport properties by studying incommensurate double-wall tubes as a simplest but representative example.

The structure of double-wall tubes has two features. One is that the lattices of outer and inner tubes are incommensurate. That is, the ratio between the periods of the outer and inner tubes in the axis direction is irrational, indicating that there is no translational symmetry in the system.[2,3] The other is that the distance between the tubes is about 3.6 Å,[4] which is almost independent of the tube radius and larger than the layer distance of graphite known as 3.35 Å. It is considered that multiwall tubes have the similar features. Therefore, intertube transfer of electrons in multiwall tubes is expected to be smaller than in graphite. However, the incommensurate lattice makes the intertube transfer a difficult problem.

Experimental results on the electrical transport of an individual multiwall tube remain very controversial. A conductance quantization was observed indicating ballistic transport although the quantized value is a half of the expected value.[5] A more recent measurement gave a quantized value in agreement with the expectation.[6] The diffusive behavior and corresponding weak-localization effects were observed more commonly.[7–9] The conductance due to intertube transfer was directly measured in telescoping multiwall tubes.[10,11]

Theoretically, special cases of commensurate armchair or zigzag double- and multiple-wall tubes have been studied intensively. It was shown that degeneracy is lifted for some energy bands and in less symmetric tubes small pseudogaps open, which sometimes leads to reduction of the number of conducting channels.[12–15] In double-wall tubes consisting of an infinitely long outer tube and a finite inner tube and in telescoping tubes, antiresonance of conducting channels with some quasibound states was shown to cause large conductance oscillations.[15–18]

For more realistic incommensurate tubes, on the other hand, calculations of electronic states[19,20] and transport properties[21–24] reported so far seem to show that intertube transfer is small. It was suggested that this is due to difference between crystal momenta of states of inner and outer tubes.[22] A similar mechanism of suppression of intertube transfer was also suggested in studies on carbon-nanotube ropes[25] and crossed carbon nanotubes.[26]

In this paper, the intertube conductance is studied in double-wall tubes with incommensurate lattice structure being fully taken into account. The paper is organized as follows. In Sec. II our model and method are introduced. Numerical results are shown in Sec. III and discussed in Sec. IV. Summary and conclusion are given in Sec. V.

II. MODEL AND METHOD

A. Tight-binding model

A tight-binding model with π orbital is used. A double-wall tube consists of an outer tube (tube 1) and an inner tube (tube 2). Each tube is modeled by a two-dimensional (2D) graphite with a periodic boundary condition in the circumference direction.

Figure 1 shows schematic illustrations of (a) a 2D graphite and (b) a carbon nanotube. We define the $x'y'$ coordinates on the 2D graphite in Fig. 1(a) and the xy coordinates for the tube in Fig. 1(b) where the x axis is along the circumference direction and the y axis is along the tube-axis direction. As shown in Fig. 1(a) primitive lattice vectors are chosen as $\mathbf{a}=a(1,0)$ and $\mathbf{b}=a(-1/2,\sqrt{3}/2)$ and three vectors which con-

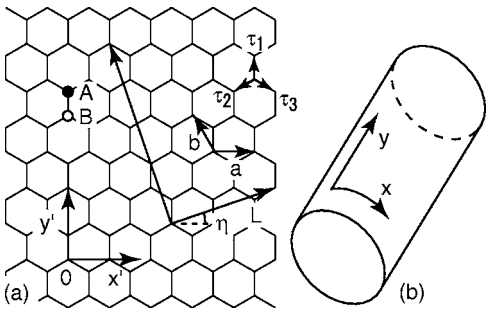

FIG. 1. Schematic illustrations of (a) a 2D graphite and (b) a carbon nanotube.

nect neighboring two sites are introduced as $\tau_1=a(0,1/\sqrt{3})$, $\tau_2=a(-1/2,-1/2\sqrt{3})$, and $\tau_3=a(1/2,-1/2\sqrt{3})$, where a is the lattice constant of the 2D graphite. A unit cell of the 2D graphite includes two sites A and B. Every tube can be specified by a chiral vector $\mathbf{L}=n_a\mathbf{a}+n_b\mathbf{b}$ with n_a and n_b being integers. Let $n_1=n_a-n_b$ and $n_2=n_b$ or $n_a=n_1+n_2$ and $n_b=n_2$. Then, the tube is usually called the (n_1,n_2) tube. In the following we shall use this convention.

A wave function ψ_1 of tube 1 satisfies the following Schrödinger equation:

$$E\psi_1(\mathbf{R}_1) = -\gamma_0 \sum_{l=1}^{3} \psi_1(\mathbf{R}_1 \mp \tau_l) - \sum_{\mathbf{R}2} t(\mathbf{R}_1,\mathbf{R}_2)\psi_2(\mathbf{R}_2), \tag{1}$$

where the upper and lower signs correspond to A and B sites of tube 1, respectively, $\psi_2(\mathbf{R}_2)$ is the wave function of tube 2 at $\mathbf{R}_2$, E the eigenenergy, $-\gamma_0$ the intratube resonance integral between the nearest-neighbor sites, and $-t(\mathbf{R}_1,\mathbf{R}_2)$ the intertube resonance integral between sites $\mathbf{R}_1$ and $\mathbf{R}_2$. In Eq. (1) the energy of a π orbital is chosen as the origin. The equation for tube 2 is similarly obtained.

The intertube resonance integral $-t(\mathbf{R}_1,\mathbf{R}_2)$ is chosen as[23,26,27]

$$\begin{aligned} -t(\mathbf{R}_1,\mathbf{R}_2) = {} & \alpha\gamma_1 \exp\left(-\frac{d-c/2}{\delta}\right)\left(\frac{\mathbf{p}_1\cdot\mathbf{d}}{d}\right)\left(\frac{\mathbf{p}_2\cdot\mathbf{d}}{d}\right) \\ & - \gamma_0 \exp\left(-\frac{d-a_0}{\delta}\right) \\ & \times[(\mathbf{p}_1\cdot\mathbf{e})(\mathbf{p}_2\cdot\mathbf{e}) + (\mathbf{p}_1\cdot\mathbf{f})(\mathbf{p}_2\cdot\mathbf{f})], \end{aligned} \tag{2}$$

where a_0 is the distance between neighboring carbons in 2D graphite given by $a_0/a=1/\sqrt{3}$, c the lattice constant along the c axis in graphite given by $c/a=2.72$, and δ the decay rate of π orbital. Further, γ_1 is the resonance integral between nearest-neighbor sites of neighboring layers.[28,29] Vectors $\mathbf{p}_1$ and $\mathbf{p}_2$ are unit vectors directed along π orbitals at $\mathbf{R}_1$ and at $\mathbf{R}_2$, respectively, $\mathbf{d}$ a vector connecting the two sites, and $\mathbf{e}$ and $\mathbf{f}$ unit vectors perpendicular to $\mathbf{d}$ and to each other.

In the following numerical calculations we use parameters $\delta/a=0.185$,[19] $\gamma_1/\gamma_0=0.119$,[30] and $\alpha=1.4$. The value of α is chosen by fitting the energy dispersion of graphite in the c-axis direction calculated with the use of Eq. (2) to that in the effective model.[28,29] Since the intertube resonance integral Eq. (2) follows exponential decay with the short decay length δ, intertube transfer into those of the other tube lying near the site is important.

In this paper we consider double-wall tubes with metallic outer and inner tubes near the Fermi energy in the undoped case. Conductance between the inner tube and the outer tube due to intertube transfer is calculated in two systems. One is a two-terminal system illustrated in Fig. 2(a) and the other is a four-terminal system in Fig. 2(b). In the latter system, intertube transfer is present only in the hatched double-wall region with length A, while tubes are independent outside the region and connected to reservoirs.

The four-terminal system is very advantageous to theoretical analysis of effects of intertube transfer itself, while the two-terminal system is similar to the telescoping tubes used in Ref. 11. As will be demonstrated in the following, intertube electron-transfer is extremely small and therefore the most of incident wave is reflected back at the tube edge in its presence. In the two-terminal geometry, the amplitudes of both incident waves and transmitted waves exhibit a strong spatial variation due to interferences caused by the edges and the presence of evanescent waves decaying exponentially away from the edges are likely to play significant roles. As a result, the intertube conductance is modified drastically by such a change in the wave function. In the four terminal geometry, on the other hand, both incident and transmitted waves have amplitude uniform in space and therefore the information on intertube transfer can be obtained directly.

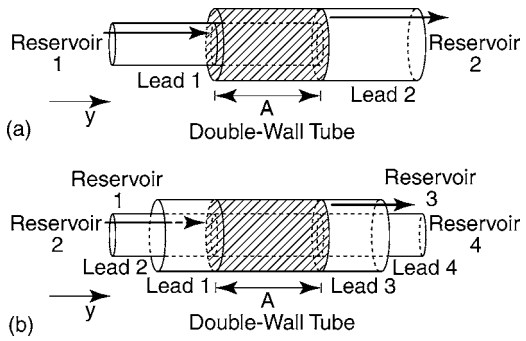

FIG. 2. Schematic illustrations of (a) a two-terminal tube and (b) a four-terminal tube. Intertube transfer is considered only in hatched double-wall regions with length A. The tube-axis direction is chosen as the y direction. Arrows indicate current flow for which the conductance is calculated.

Calculation of conductance for long tubes requires a recursive Green's function technique.[31] Because the lattice structure of an inner and outer tube is incommensurate, the most complicated (time consuming also) procedure lies in the generation of a Hamiltonian matrix in each recursion step. In order to avoid this complication and make the calculation process much smoother, we shall restrict ourselves to a nanotube with a set of edges selected beforehand.

For this purpose a unit cell is separated into columns in such a way that the number of atoms in each column is the same as that of independent modes (going in the positive y direction, for example) of the tube and that each atom is connected through bonds to those in the neighboring columns in both sides. Figure 3 shows columns for (1,4), (4,7), and (7,4) nanotubes. This separation is usually not possible for all atoms contained in a unit cell and therefore remaining isolated atoms are absorbed into the column lying in the right hand side. Each column in a unit cell will be denoted by integer m in the following. It is clear that there can be many different ways of separation of a unit cell into columns.

In each recursive step several columns are combined to form a segment. The segment size, i.e., the number of columns, should be determined such that only intratube and intertube couplings between nearest neighbor segments are present and couplings between other segments can be neglected completely. For an outer tube the number of columns in a segment is fixed as N, while in an inner tube is chosen as $N+1$ or $N-1$ depending on the inner tube is shorter or longer

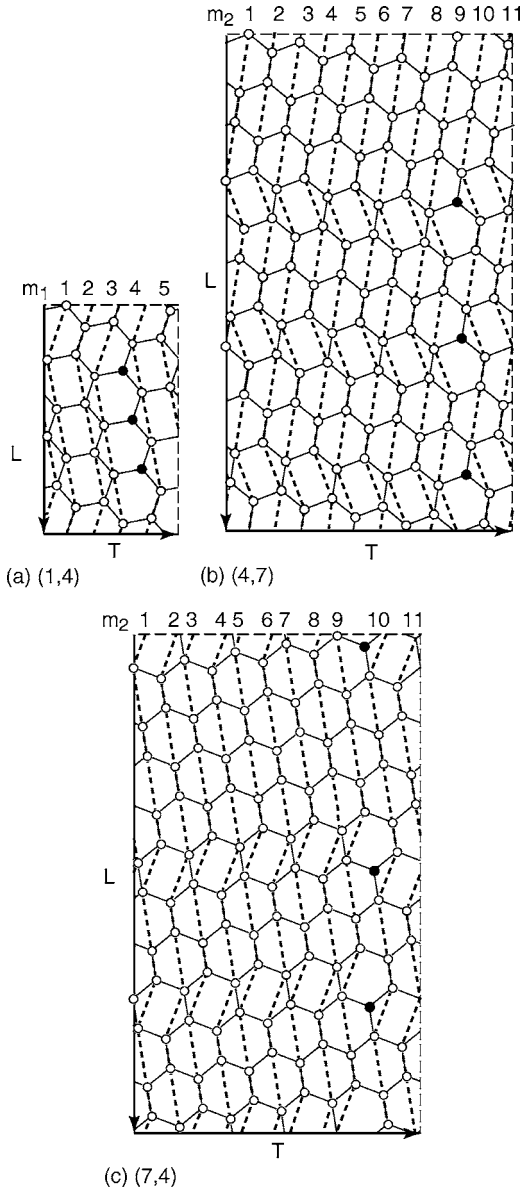

FIG. 3. Unit cells of (a) (1,4), (b) (4,7), and (c) (7,4) tubes and their separation into columns. Isolated sites are denoted by a closed circle.

than the outer tube in the previous recursive step. In this way we can generate uniform length distribution between inner and outer tubes.

The boundary of the double-wall region is given by the edge of the first segment at the left edge and that of the final segment added after each step of the recursion at the right edge. Therefore, the left edge is fixed and the right edge changes as a function of the length. The length of each tube is defined by $A_i = N_i(\sqrt{3}a^2/4)/L_i$ with $i=1,2$ where N_i is the number of carbon atoms in the double-wall region of tube i. The length of the double-wall region is defined by a geometric mean $A=\sqrt{A_1 A_2}$.

Using Landauer's formula,[32] the conductance is given by

$$G = \frac{e^2}{\pi\hbar}\sum_{\mu,\nu}|S_{\mu\nu}|^2, \tag{3}$$

where $S_{\mu\nu}$ is the scattering matrix describing transmission from a channel ν to a channel μ. For the current flowing from the left lead of the inner tube to the right lead of the outer tube as shown in Fig. 2, for example, the summation is taken over channels with positive velocities in the inner tube and those in the outer tube.

B. Lowest-order approximation

Consider the four-terminal geometry. Near the Fermi energy, a metallic single-wall tube has four states in the vicinity of the $\mathbf{K}$ and $\mathbf{K}'$ points with wave vectors $\mathbf{K}=(2\pi/a)\times(1/3,1/\sqrt{3})$ and $\mathbf{K}'=(2\pi/a)(2/3,0)$ at the corners of the hexagonal first Brillouin zone of 2D graphite. They are right-going states with positive velocities $\psi^{K(+)}$ and $\psi^{K'(+)}$, and left-going states with negative velocities $\psi^{K(-)}$ and $\psi^{K'(-)}$. In order to make system-size dependence clear, we shall choose the normalization in such a way that the amplitude of these traveling waves is unity at each site.

The matrix element of intertube transfer between state ψ_1^μ of tube 1 and ψ_2^ν of tube 2 is written as

$$V_{\mu\nu} = \frac{1}{\sqrt{N_1 N_2}}\sum_{\mathbf{R}_1}\sum_{\mathbf{R}_2} t^{\mu\nu}(\mathbf{R}_1,\mathbf{R}_2), \tag{4}$$

with

$$t^{\mu\nu}(\mathbf{R}_1,\mathbf{R}_2) = \psi_1^\mu(\mathbf{R}_1)^* t(\mathbf{R}_1,\mathbf{R}_2)\psi_2^\nu(\mathbf{R}_2). \tag{5}$$

In the lowest order approximation, the corresponding scattering matrix is given by

$$S_{\mu\nu} = -i\frac{A}{\hbar\sqrt{|v_\mu v_\nu|}}V_{\mu\nu}, \tag{6}$$

where v_μ and v_ν are the velocities of states μ and ν, respectively. Exactly at $\mathbf{K}$ and $\mathbf{K}'$ points we have $|v_\mu|=|v_\nu|=\gamma/\hbar$ with $\gamma=(\sqrt{3}/2)a\gamma_0$.

At the Fermi energy, ψ^μ is given by

$$\psi^\mu(\mathbf{R}) = \exp(i\mathbf{k}\cdot\mathbf{R} + i\phi), \tag{7}$$

where $\mathbf{k}=\mathbf{K}$ or $\mathbf{K}'$ and ϕ is a phase dependent on $\mathbf{K}$ or $\mathbf{K}'$ points, A or B sites, and the sign of the group velocity. In particular, the relative phase at A and B sites varies between right- and left-going waves, giving rise to difference between transition probabilities into two directions.

Because the parameter γ_1 dominantly determining intertube transfer at each site is much smaller than γ_0 the scattering matrix is approximated quite well by Eq. (6) when the region is not so large, as has been shown in the case of crossed nanotubes.[26] Further, the lowest-order expression continues to be valid if $V_{\mu\nu}$ remains small even with the increase of the region.[33,34] As will be demonstrated below, this is always the case in incommensurate nanotubes.

III. NUMERICAL RESULTS

In the following we shall show results for double-wall tubes consisting of an outer (4,16) tube [with a unit cell four

times as large as that of the (1,4) tube] and an inner (4,7) or (7,4) tube as typical results among about a hundred double-wall tubes studied. They will be called $(4,16)/(4,7)$ and $(4,16)/(7,4)$ tubes in the following. Separations of unit cells into columns are shown in Fig. 3. The left boundary of the outer and inner tube is chosen as $m=1$. We use $N=6$ as the number of columns for one segment in outer tubes in the recursive Green's function method. Further, the probability of the transmission from the left inner tube to the right outer tube will be discussed exclusively in the four-terminal geometry. The other transmission probabilities are discussed in the next section.

A. Intertube conductance

Figures 4(a) and 4(b) show conductance in the lower panels and its average $\langle G \rangle$ and fluctuation ΔG in the upper panels for $(4,16)/(4,7)$ and $(4,16)/(7,4)$ tubes, respectively. The length is measured in units of the circumference of the outer tube $L_1/a=4\sqrt{21}$. The results show that the conductance remains much smaller than $e^2/\pi\hbar$ and exhibits a wild and irregular oscillation as a function of the length. Its average and fluctuation, however, are independent of the length. This behavior continues up to nanotubes with realistic length of about 10 μm.

Figure 5 compares the exact conductance plotted by squares with that calculated in the lowest-order approximation plotted by crosses for short nanotubes. It is clear that the lowest-order approximation can reproduce the length dependence of the conductance almost exactly when the tube length is sufficiently short. As has been discussed in Sec. II B, intertube transfer at each site is much smaller than intratube transfer γ_0 and therefore the scattering matrix is approximated quite well by $V_{\mu\nu}$. Figure 5 means that $V_{\mu\nu}$ remains small even with the increase of the region, showing that intertube transfers at different sites tend to cancel each other when being summed up.

Figure 6 shows the conductance calculated in the lowest-order approximation for the same system as that in Fig. 4(a). In Fig. 7 distributions of conductance in Figs. 4(a) and 6 are plotted by a solid and dotted lines, respectively. These two figures show that the lowest-order approximation works well even for very long nanotubes. In fact, the average and fluctuation of the conductance are in agreement between these results within 1%.

B. Oscillation of inter-tube transfer

In order to understand the behavior of the intertube conductance we shall define an effective intertube coupling of a site $\mathbf{R}$ in tube 1 with tube 2 by

$$t^{\mu\nu}(\mathbf{R}) = \sum_{\mathbf{R}_2} t^{\mu\nu}(\mathbf{R},\mathbf{R}_2), \tag{8}$$

where $t^{\mu\nu}(\mathbf{R},\mathbf{R}_2)$ is given in Eq. (5) and the summation is over all sites in the double-wall region of tube 2.

Figures 8(a) and 8(b) show the real part of effective intertube couplings for a $(4,16)/(7,4)$ tube, $t^{K(+)K(+)}(\mathbf{R})$ and $t^{K(+)K'(+)}(\mathbf{R})$, respectively, as functions of the y coordinate.

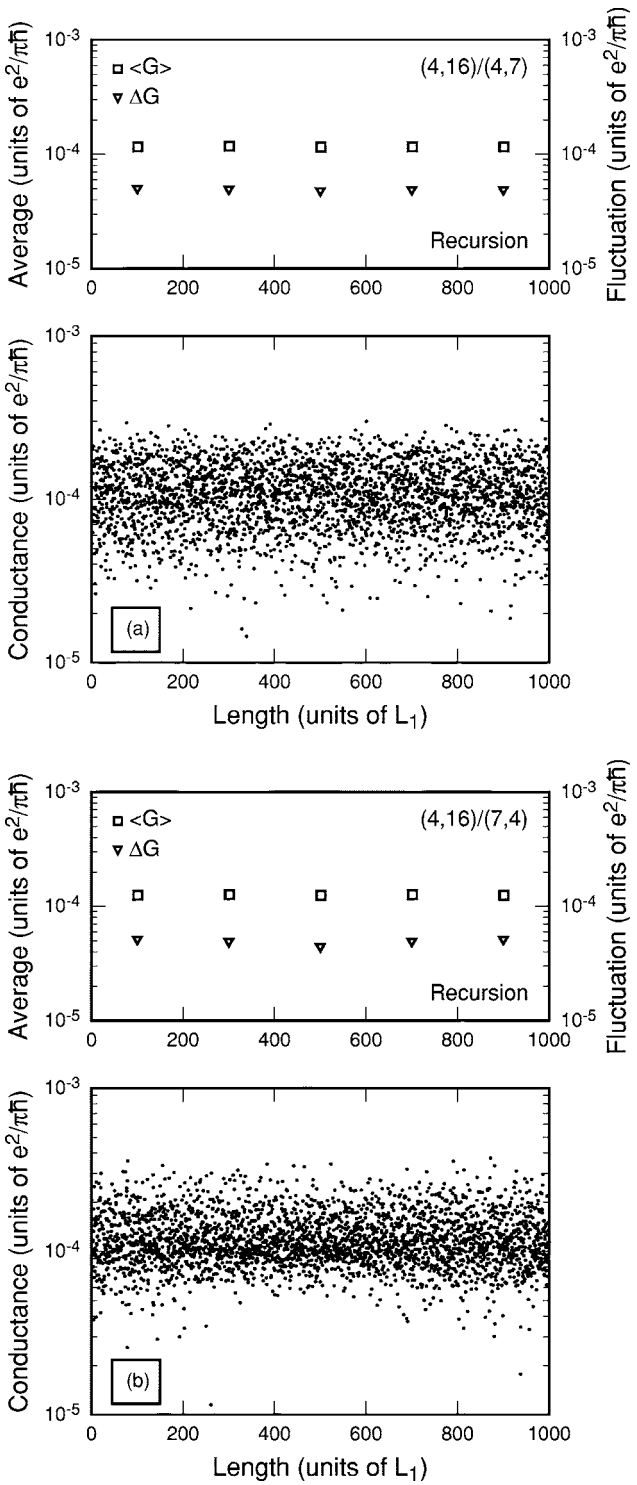

FIG. 4. The conductance in lower panels and its average and fluctuation in upper panels for the four-terminal (a) $(4,16)/(4,7)$ and (b) $(4,16)/(7,4)$ tubes. The averages and fluctuations are calculated for $200n \leqslant A/L_1 < 200(n+1)$ with $n=0,1,\ldots$, where A is the length of the double-wall region and L_1 is the circumference of the outer tube.

They exhibit complex oscillations around the origin. The imaginary part of $t^{K(+)K(+)}(\mathbf{R})$ and $t^{K(+)K'(+)}(\mathbf{R})$ and the other components $t^{K'(+)K(+)}(\mathbf{R})$ and $t^{K'(+)K'(+)}(\mathbf{R})$ exhibit the similar behavior.

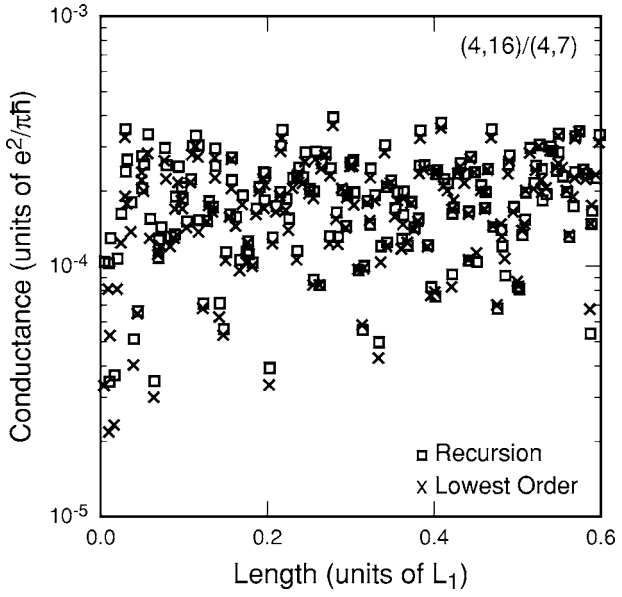

FIG. 5. The conductance calculated in the recursion method (squares) and the lowest-order approximation (crosses) for the four-terminal $(4,16)/(4,7)$ tubes with short length.

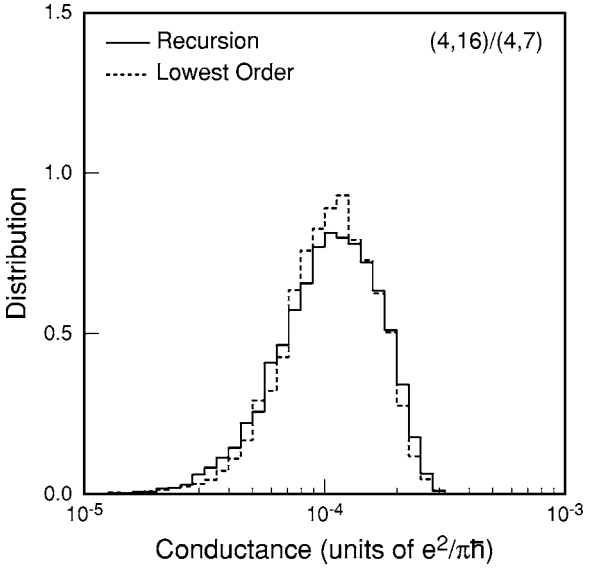

FIG. 7. Conductance distributions for four-terminal $(4,16)/(4,7)$ tubes. A solid line is calculated in the recursion method and dotted in the lowest-order approximation.

The effective intertube couplings $t^{K(+)K(+)}(\mathbf{R})$ and $t^{K(+)K'(+)}(\mathbf{R})$ in Fig. 8 are plotted in complex planes in Figs. 9(a) and 9(b), respectively. They are scattered on some regions whose centers of mass are close to the origin. The amplitude is of the order of $0.1\gamma_0$ which is much smaller than γ_0. When the tube length is increased, the effective intertube couplings densely cover the area enclosed by envelopes of the points and its average over position $\mathbf{R}$ decreases in proportion to the inverse of the length [$(\sim 10^{-6}\times \gamma_0(L_1/A)$ in a $(4,16)/(7,4)$ tube].

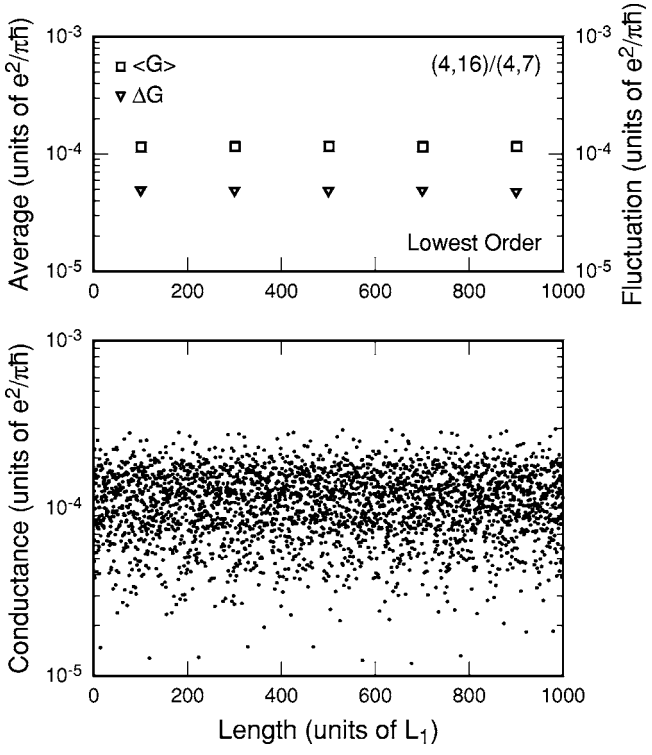

FIG. 6. The conductance in a lower panel and its average and fluctuation in a upper panel for four-terminal $(4,16)/(4,7)$ tube, calculated in the lowest-order approximation. The averages and fluctuations are calculated for $200n \leqslant A/L_1 < 200(n+1)$ with $n=0,1,\ldots$.

The phase of the wave function in Eq. (7) jumps by an amount $\pm 2\pi/3$ when the position changes by a primitive lattice vector. Because of this rapid phase jump and the quasiperiodic nature due to incommensurate lattice structure, almost all intertube transfers cancel out in Eq. (4) and remain nonzero only because of an incomplete cancellation due to the presence of sharp edges. The situation is analogous to a series of numbers with alternating signature with an equal absolute value $(+1,-1,+1,\ldots$, for example). When the number of terms in the summation increases, such a series does not converge but oscillates with an average and fluctuation independent of the number of terms.

For rapidly oscillating intertube transfers most probable amplitude of matrix elements of intertube transfer in Eq. (4) is given by the fluctuation of effective intertube coupling, i.e.,

$$|V_{\mu\nu}| \approx \frac{1}{\sqrt{N_1 N_1}} \sqrt{\langle |t^{\mu\nu}(\mathbf{R})|^2 \rangle}, \tag{9}$$

which gives

$$\langle G \rangle \approx \frac{e^2}{\pi\hbar} \frac{a^2}{L_1 L_2} \frac{\langle |t^{\mu\nu}(\mathbf{R})|^2 \rangle}{\gamma_0^2} \tag{10}$$

with the use of Eq. (6). This is independent of the length A and also gives $\langle G \rangle \sim 10^{-4} \times (e^2/\pi\hbar)$ for $\sqrt{\langle |t^{\mu\nu}(\mathbf{R})|^2 \rangle}/\gamma_0 \sim 0.1$ in order-of-magnitude agreement with the calculated average conductance for $(4,16)/(7,4)$ and $(4,16)/(4,7)$ tubes.

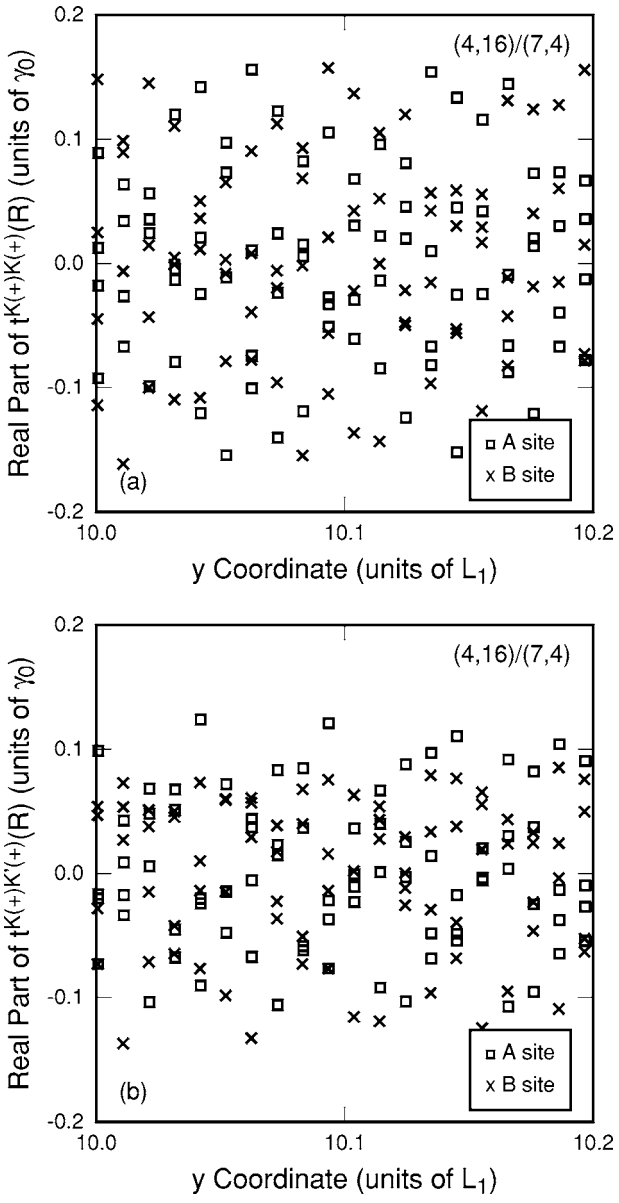

FIG. 8. Dependence of the real part of effective intertube couplings on the y coordinate for $(4,16)/(7,4)$ tube, (a) $t^{K(+)K(+)}(\mathbf{R})$ and (b) $t^{K(+)K'(+)}(\mathbf{R})$. Squares are results at A sites and crosses those at B sites.

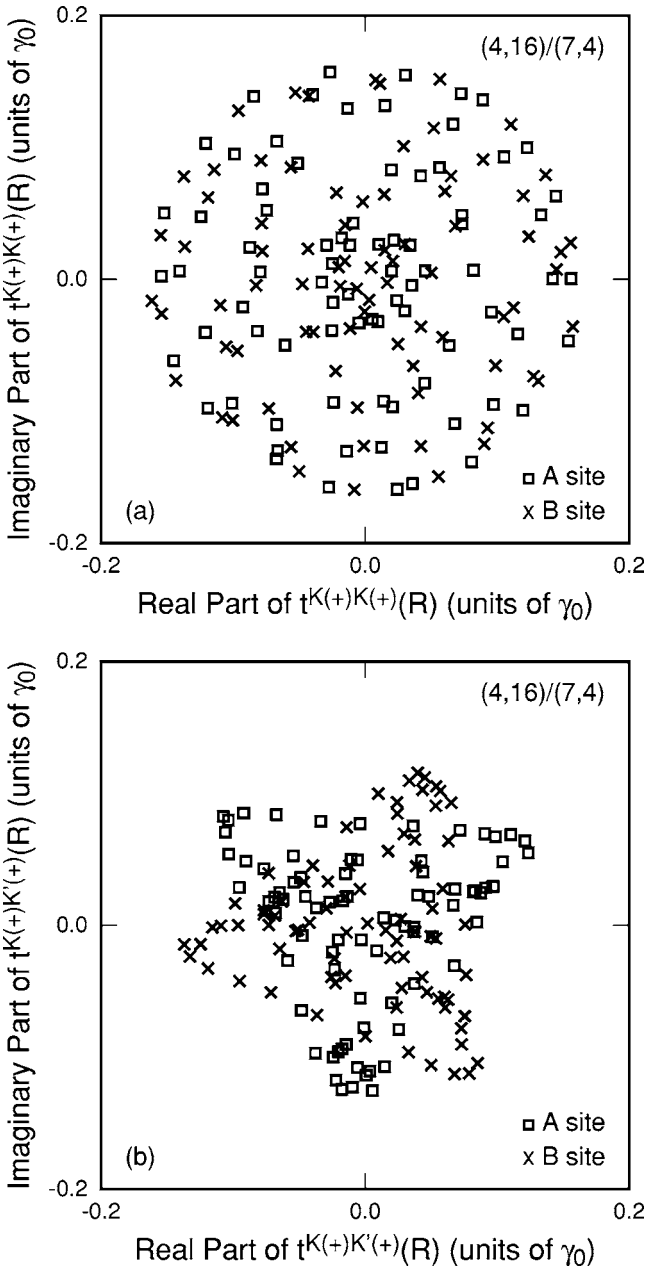

FIG. 9. The intertube transfer (a) $t^{K(+)K(+)}(\mathbf{R})$ and (b) $t^{K(+)K'(+)}(\mathbf{R})$ for $(4,16)/(7,4)$ tube in complex planes for $10 \leqslant y/L_1 \leqslant 10.2$. Squares are results at A sites and crosses those at B sites.

C. Edge effects

The present reasoning leads to the conclusion that the intertube conductance is extremely sensitive to the structure of edges. Figure 10 shows the distribution function of the conductance for $(4,16)/(4,7)$ and $(4,16)/(7,4)$ tubes with three different edges. The solid lines are the results for the same systems as those in Fig. 4. The dotted lines are results for the tubes where left edges are chosen as $m=2$ and 6 for the outer and inner tube, respectively. A dashed line is the result for tubes with straight edges that are defined by two straight lines with distance A, obtained in the lowest-order approximation (there is no essential complication in dealing with arbitrary edges within the lowest approximation).

The figure clearly demonstrates the strong dependence of the intertube conductance on the structure of edges. Further, this edge dependence is sensitive to the structure of the nanotube also. In fact, the dashed line is shifted to the right-hand side of the solid line in (a), but to the left-hand side in (b).

In order to demonstrate importance of sharp edges, further, we make edges smoother by multiplying the intertube resonance integral Eq. (2) by the following function:

$$F(y) = \frac{1}{2}\left[1 - \mathrm{erf}\left(\frac{|y| - \frac{1}{2}A}{\Delta}\right)\right], \tag{11}$$

with $\mathrm{erf}(y)$ being the error function defined by

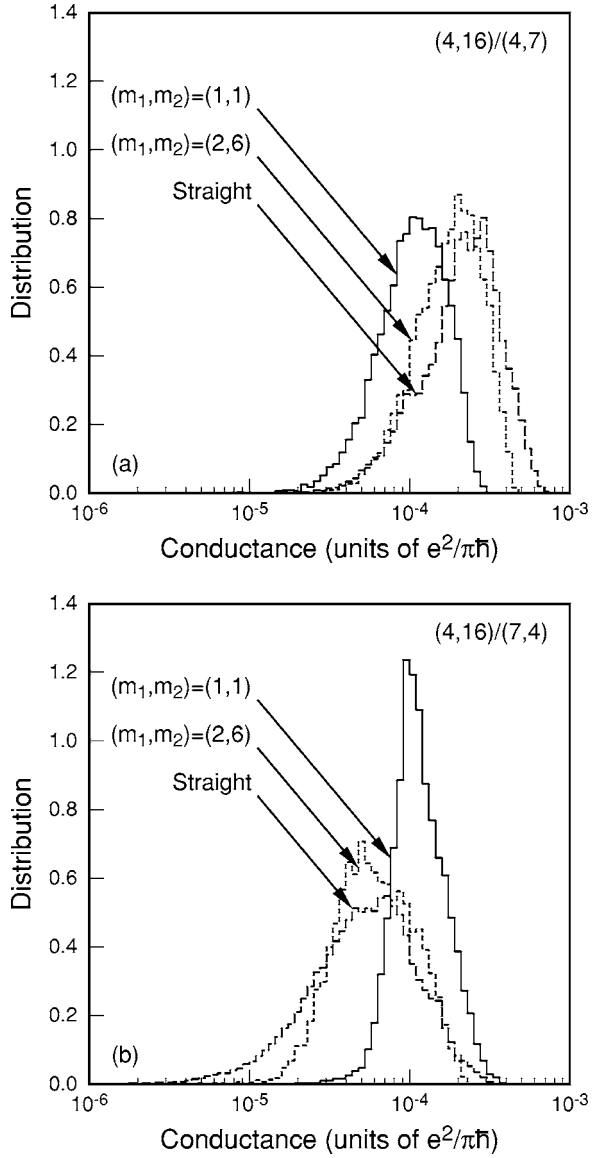

FIG. 10. Conductance distributions for (a) $(4,16)/(4,7)$ and (b) $(4,16)/(7,4)$ tubes with three different edges. For solid and dotted lines the left edges consist of columns specified by $(m_1,m_2)=(1,1)$ and (2,6), respectively, while for dashed lines both edges are given by vertical straight lines. The solid and dotted liens are calculated in the recursion method and the dashed lines in the lowest-order approximation.

$$\mathrm{erf}(y) = \frac{2}{\sqrt{\pi}} \int_0^y e^{-t^2} dt, \tag{12}$$

where $y=(y_1+y_2)/2$ with y_1 and y_2 being the y coordinate of sites in outer and inner tubes, respectively, and A is the effective tube length. This function gradually increases or decreases the intertube coupling over the range Δ.

Figure 11 shows the dependence of the conductance for $(4,16)/(7,4)$ tubes on Δ, obtained in the lowest-order approximation. With the increase of Δ the conductance rapidly decreases and becomes more than three order of magnitude smaller for $\Delta/a \sim 1$ than that for $\Delta/a=0$. All these results

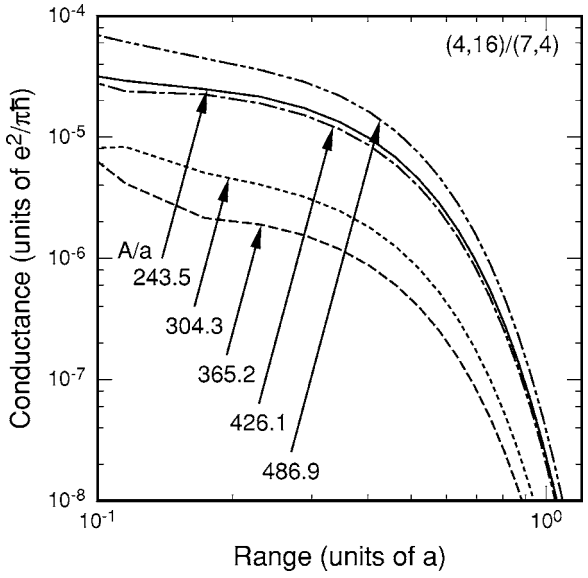

FIG. 11. Dependence of conductance for $(4,16)/(7,4)$ tubes on the range Δ, calculated in the lowest-order approximation. Results for five different values of the length $A/a \approx 243.5$, 304.3, 365.2, 426.1, and 486.9, are shown.

show that detailed information on edges is necessary for the accurate prediction on the value of the intertube conductance because a slight change in edge configurations leads to an order-of-magnitude difference.

D. Two-terminal system

Figure 12 shows the length dependence of the conductance in the lower panel and that of the average and fluctuation in the upper panel in the two-terminal $(4,16)/(7,4)$ tubes, obtained using recursive Green's function technique. The system is same as that shown in Fig. 4(b) except for the presence of the edges. The result is qualitatively same as the conductance in the four-terminal systems. However, there is a significant quantitative difference. In fact, the average $2.2\times10^{-3}e^2/\pi\hbar$ is about twenty times and the fluctuation $2.8\times10^{-3}e^2/\pi\hbar$ is about sixty times as large as that of the four-terminal system shown in Fig. 4(b).

This quantitative difference is mainly attributed to waves reflected at the tube edges. In the two terminal system states of each tube in the absence of intertube transfer become standing waves with the maximum amplitude twice as large as that of traveling waves. Then it is possible that the intertube coupling oscillates as a function of position with an amplitude four times as large as that for the four-terminal system. Taking account of a factor $1/2$ which arises from an average of squared absolute values of oscillating intertube coupling, the conductance can become eight times as large as that for the four-terminal system.

Because boundary conditions at edges cannot be satisfied by traveling waves alone, the wave function contains many evanescent modes decaying exponentially away from edges. Such evanescent modes sensitive to the structure of the edge tend to increase or reduce intertube transfer in the vicinity of edges considerably and therefore can strongly modify the

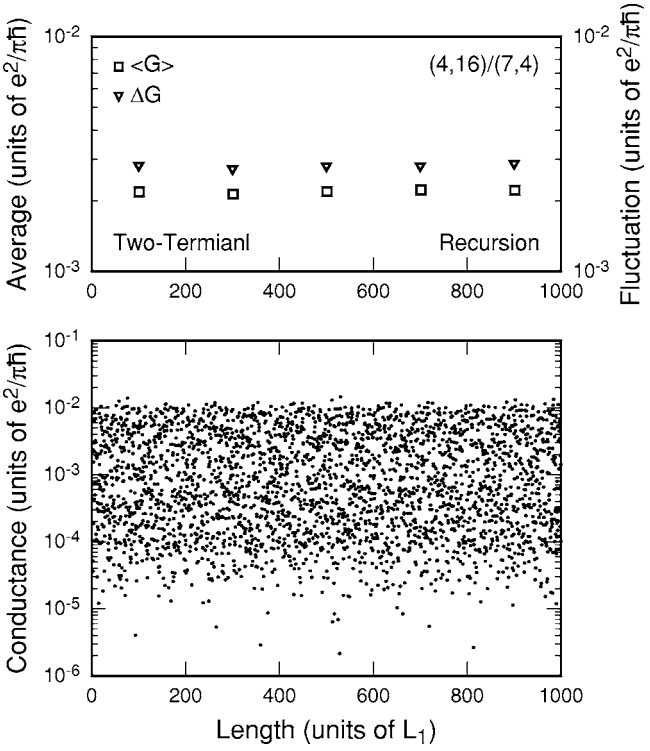

FIG. 12. The conductance in a lower panel and its average and fluctuation in a upper panel in the two-terminal $(4,16)/(7,4)$ tubes. The average and fluctuation are calculated for $200n \leqslant A/L_1 < 200(n+1)$ with $n=0,1,\ldots$.

intertube conductance through the enhancement of the incomplete cancellation of intertube transfers. Therefore, the enhancement of the average and fluctuation of the conductance more than one-order-of-magnitude is to be expected.

IV. DISCUSSION

For sufficiently small energy, the effective-mass approximation or $\mathbf{k}\cdot\mathbf{p}$ scheme provides an accurate description of the wave functions.[35] It shows that the wave functions at A and B sites change their relative phase by π between right- and left-going states in the vicinity of the $\mathbf{K}$ point and that the same is applicable in the vicinity of the $\mathbf{K}'$ point. As a result, the probability of transmission to the left outer tube and to the right outer tube are different for the electron injection from the left inner tube in the four-terminal system. Numerical results, although not shown explicitly here, show that these transmission probabilities exhibit almost same statistical behavior. They show also that the reflection probability is approximately of the order of that of inter-tube transmission although it can be larger or smaller depending on the structure. Therefore, almost all electrons transmit through the incident tube ballistically. This is certainly the same for the injection into the outer tube and consistent with the observation of a conductance quantization in multiwall nanotubes.[6]

As mentioned already, explicit calculations have been performed for nearly a hundred different double-wall nanotubes with incommensurate lattice structure. It is found that in some exceptional incommensurate tubes [for example, $(6,15)/(1,10)$ and $(10,16)/(5,11)$] the conductance can be as large as the conductance quantum. The actual development map of tubes should be drawn in such a way that the circumference of the inner and outer tube agrees with each other by changing the scale appropriately. It is possible that in such a deformed map lattices of outer and inner tube happen to be nearly commensurate over a wide area. This kind of accidental near-commensurability occurs only in very rare occasions, however (several percents among the tubes considered).

For such exceptional nanotubes the conductance obtained in the lowest-order approximation deviates from the recursive result considerably. Even for nanotubes with small average conductance the lowest-order conductance can deviate from the exact result with the increase of the length. The reason is that there can be some spatial regions where the intertube transfer can be as large as γ_0 when being summed over and the lowest-order approximation becomes inappropriate, depending on the structure sensitively. Further, higher-order contributions, however, small they might be, can be accumulated for very long tubes and therefore give observable contributions due to the cancellation of the intertube coupling. In fact, a careful comparison between Figs. 4(a) and 6 reveals that the lowest-order approximation fails to reproduce the exact conductance value at each length. However, the overall statistical behavior, including the distribution function of the conductance, is almost always reproduced by the lowest-order approximation quite well.

The average of the intertube conductance has been shown to be independent of the length and is approximately described by Eq. (10). This equation shows that the intertube conductance decreases with the circumference or the diameter in proportion to the inverse of the square of the circumference. Indeed, numerically calculated conductance shows the tendency that the conductance decreases with increase of tube diameter although the exact dependence is not determined due to the limitation of computational time for tubes with large diameter.

At nonzero temperature the presence of phase-breaking scattering giving a finite phase coherence length L_ϕ should be considered. One way to take into account this effect is to separate the nanotube into segments with length of the order of the phase coherence length and assume that the electron looses the phase information after transmission through each segment.[36] In this case intertube transfer occurs in each segment with a probability independent of the length as has been obtained above. Because intertube transfer is incoherent between different segments, the conductance becomes proportional to the number of such segments, i.e., $G \propto A/L_\phi$, where A is the length of the double-wall region. Using a phase coherence length of 300 nm at about 10 K obtained experimentally[9] and the average conductance of $10^{-3}e^2/\pi\hbar$, we need $A=3$ mm to have the conductance of the order of $e^2/\pi\hbar$.

The present result that intertube transfer is small in incommensurate double-wall tubes is consistent with the results of other theoretical studies.[22,25,26] However, our finding that the averaged intertube conductance is independent of tube length is quite in contrast to a power-law decay for the comparable length suggested previously.[22] A similar power-

law decay may be obtained by replacing $\sqrt{\langle|t^{\mu\nu}(\mathbf{R})|^2\rangle}$ by $|\langle t^{\mu\nu}(\mathbf{R})\rangle|$ incorrectly in Eq. (9), giving a conductance proportional to inverse of square of the length.

It is known that the wave function sometimes decays following a power law in one- and two-dimensional quasiperiodic systems.[37–39] The similar behavior is likely to appear and the intertube conductance may eventually exhibit a certain power-law dependence when incommensurate double-wall nanotubes become much longer than those studied here. The present results show, however, that such a power-law decay does not occur in realistic tubes with lengths of a few tens micrometers.

The large conductance fluctuation as a function of the length originates from the discrete change in the edge. In the calculations presented above, we have introduced a sharp edge for both inner and outer tubes and achieved the length change by adding or removing carbon atoms at an edge. The effective intertube coupling of these atoms exhibits discrete jumps as has been discussed in Sec. III B, leading to the large fluctuation. In actual double-wall nanotubes similar to that shown in Fig. 2(a), the left edge of the outer tube is well defined, but that of the inner tube is broadened over the distance determined by the spatial extent of the π orbital. The same is applicable to the right edge. Even if such broadening is considered, the conductance exhibits fluctuations of the same amount as long as the length of the double-wall region changes by adding or subtracting carbon atoms at the edge.

The situation changes when the length of the double-wall region is varied smoothly for a fixed form of the edges. In fact, the conductance changes smoothly as a function of the length with much less fluctuations. This can be demonstrated by a lowest-order calculation in the four-terminal geometry shown in Fig. 2(b) as a function of the position of the inner tube for fixed left and right edges of the outer tube. The situation is analogous to the case of crossed nanotubes, for which the intertube conductance shows no fine fluctuations as a function of the angle.[26]

In actual telescoping tubes, the conductance is measured as a function of the length with fixed edges at the left end of the outer tube and at the right end of the inner tube as shown in Fig. 2(a). It is expected, therefore, that the intertube conductance varies more smoothly without discrete fluctuations. Calculations for such tubes are certainly desirable, but are quite time consuming and left for future, because the recursive procedure is not directly applicable and even the lowest-order approximation is not possible. Without explicit calculations, however, we can say at least that the absolute value of the conductance is of the same order as obtained above $G \sim 10^{-3}(e^2/\pi\hbar)$ and remains essentially independent of the length. Measured intertube conductance[10,11] is much larger (for example, ~ 0.03 and ~ 0.3 in units of $e^2/\pi\hbar$) and therefore cannot be explained by such calculations.

In intertube transport, effects of electron-electron interaction can be important. For metallic single-wall nanotubes, low-energy properties were theoretically investigated.[40–44] In experiments characteristic power-law behavior of tunneling conductance[45,46] and the density of states[47] indicated that the system is regarded as a Tomonaga-Luttinger liquid. For multiwall nanotubes, a similar behavior was theoretically suggested,[48] but experimental results seem to depend strongly on samples and conditions.[49–53]

The present results of intertube coupling is used for the basis for analysis of such interaction effects. If multiwall tubes are described as weakly coupled Tomonaga-Luttinger liquid and intertube transfer is regarded as tunneling, the intertube conductance is likely to exhibit a power-law dependence on the temperature and bias voltage. Intertube transfer may act also as weak scatterers and cause strong backward scattering within each tube,[54] possibly leading to a suppression of the intertube transfer. Such intriguing problems are left for a future study.

V. SUMMARY AND CONCLUSION

The intertube conductance in incommensurate double-wall tubes has been numerically studied. Because the intertube transfer at each site is small and exhibits a discrete jump in a quasiperiodic manner as a function of position, it cancels out each other almost completely when being summed over many sites. The conductance appears only in the presence of sharp edges making the cancellation incomplete. As a result, the conductance oscillates as a function of the length with a length-independent small average $[\lesssim 10^{-3}(e^2/\pi\hbar)]$ and fluctuation. It is concluded that intertube transfer can be safely neglected in multiwall nanotubes.

ACKNOWLEDGMENTS

This work was supported in part by a 21st Century COE Program at Tokyo Tech "Nanometer-Scale Quantum Physics" and by a Grant-in-Aid for Scientific Research from the Ministry of Education, Culture, Sports, Science and Technology, Japan. Numerical calculations were performed in part using the facilities of the Supercomputer Center, Institute of Solid State Physics, University of Tokyo and the Advanced Computing Center, RIKEN.

*Also at Condensed-Matter Theory Laboratory, RIKEN, 2-1 Hirosawa, Wako-shi, Saitama, Japan.

[1] S. Iijima, Nature (London) **354**, 56 (1991).
[2] M. Kociak, K. Suenaga, K. Hirahara, Y. Saito, T. Nakahira, and S. Iijima, Phys. Rev. Lett. **89**, 155501 (2002).
[3] J. M. Zuo, I. Vartanyants, M. Gao, R. Zhang, and L. A. Nagahara, Science **300**, 1419 (2003).
[4] S. Bandow, M. Takizawa, K. Hirahara, M. Yudasaka, and S. Iijima, Chem. Phys. Lett. **337**, 48 (2001).
[5] S. Frank, P. Poncharal, Z. L. Wang, and W. A. de Heer, Science **280**, 1744 (1998).
[6] A. Urbina, I. Echeverría, A. Pérez-Garrido, A. Díaz-Sánchez, and

J. Abellán, Phys. Rev. Lett. **90**, 106603 (2003).
[7] L. Langer, V. Bayot, E. Grivei, J.-P. Issi, J. P. Heremans, C. H. Olk, L. Stockman, C. Van Haesendonck, and Y. Bruynseraede, Phys. Rev. Lett. **76**, 479 (1996).
[8] A. Bachtold, C. Strunk, J. P. Salvetat, J. M. Bonard, L. Forro, T. Nussbaumer, and C. Schönenberger, Nature (London) **397**, 673 (1999).
[9] C. Schönenberger, A. Bachtold, C. Strunk, J.-P. Salvetat, and L. Forró, Appl. Phys. A: Mater. Sci. Process. **69**, 283 (1999).
[10] A. Zettl and J. Cumings, in *NANONETWORK MATERIALS: Fullerenes Nanotubes, and Related Systems; ISNM 2001*, edited by Susumu Saito *et al.*, AIP Conf. Proc. No. 590 (AIP, Melville, 2001), p. 107.
[11] J. Cumings and A. Zettl, Phys. Rev. Lett. **93**, 086801 (2004).
[12] R. Saito, G. Dresselhaus, and M. S. Dresselhaus, J. Appl. Phys. **73**, 494 (1993).
[13] Y.-K. Kwon and D. Tomanek, Phys. Rev. B **58**, R16 001 (1998).
[14] S. Sanvito, Y.-K. Kwon, D. Tomanek, and C. J. Lambert, Phys. Rev. Lett. **84**, 1974 (2000).
[15] D.-H. Kim, H.-S. Sim, and K. J. Chang, Phys. Rev. B **64**, 115409 (2001).
[16] D.-H. Kim and K. J. Chang, Phys. Rev. B **66**, 155402 (2002).
[17] R. Tamura, Y. Sawai, and J. Haruyama, Phys. Rev. B **72**, 045413 (2005).
[18] T. Matsumoto and S. Saito, in *PHYSICS OF SEMICONDUCTORS: 27th International Conference on the Physics of Semiconductors*, edited by José Menéndez and Chris G. Van de Walle, AIP Conf. Proc. No. 772 (AIP, Melville, 2005), p. 1055.
[19] Ph. Lambin, V. Meunier, and A. Rubio, Phys. Rev. B **62**, 5129 (2000).
[20] K.-H. Ahn, Y.-H. Kim, J. Wiersig, and K. J. Chang, Phys. Rev. Lett. **90**, 026601 (2003).
[21] S. Roche, F. Triozon, A. Rubio, and D. Mayou, Phys. Rev. B **64**, 121401(R) (2001).
[22] Y.-G. Yoon, P. Delaney, and S. G. Louie, Phys. Rev. B **66**, 073407 (2002).
[23] S. Uryu, Phys. Rev. B **69**, 075402 (2004).
[24] F. Triozon, S. Roche, A. Rubio, and D. Mayou, Phys. Rev. B **69**, 121410(R) (2004).
[25] A. A. Maarouf, C. L. Kane, and E. J. Mele, Phys. Rev. B **61**, 11156 (2000).
[26] T. Nakanishi and T. Ando, J. Phys. Soc. Jpn. **70**, 1647 (2001).
[27] J. C. Slater and G. F. Koster, Phys. Rev. **94**, 1498 (1954).
[28] J. W. McClure, Phys. Rev. **108**, 612 (1957).
[29] J. C. Slonczewski and P. R. Weiss, Phys. Rev. **109**, 272 (1958).
[30] H. Nagayoshi, K. Nakao, and Y. Uemura, J. Phys. Soc. Jpn. **41**, 1480 (1976).
[31] T. Ando, Phys. Rev. B **44**, 8017 (1991).
[32] R. Landauer, IBM J. Res. Dev. **1**, 223, (1957); Philos. Mag. **21**, 863 (1970).
[33] M. Igami, T. Nakanishi, and T. Ando, Mol. Cryst. Liq. Cryst. Sci. Technol., Sect. A **340**, 719 (2000).
[34] T. Ando, T. Nakanishi, and M. Igami, J. Phys. Soc. Jpn. **68**, 3994 (1999).
[35] T. Ando, J. Phys. Soc. Jpn. **74**, 777 (2005).
[36] T. Ando and H. Suzuura, J. Phys. Soc. Jpn. **71**, 2753 (2002).
[37] M. Kohmoto, L. P. Kadanoff, and C. Tang, Phys. Rev. Lett. **50**, 1870 (1983).
[38] S. Ostlund, R. Pandit, D. Rand, H. J. Schellnhuber, and E. D. Siggia, Phys. Rev. Lett. **50**, 1873 (1983).
[39] K. Ueda and H. Tsunetsugu, Phys. Rev. Lett. **58**, 1272 (1987).
[40] L. Balents and M. P. A. Fisher, Phys. Rev. B **55**, R11 973 (1997).
[41] Yu. A. Krotov, D.-H. Lee, and S. G. Louie, Phys. Rev. Lett. **78**, 4245 (1997).
[42] R. Egger and A. O. Gogolin, Phys. Rev. Lett. **79**, 5082 (1997).
[43] C. Kane, L. Balents, and M. P. A. Fisher, Phys. Rev. Lett. **79**, 5086 (1997).
[44] H. Yoshioka and A. A. Odintsov, Phys. Rev. Lett. **82**, 374 (1999).
[45] M. Bockrath, D. H. Cobden, J. Lu, A. G. Rinzler, R. E. Smalley, L. Balents, and P. L. McEuen, Nature (London) **397**, 598 (1999).
[46] Z. Yao, H. W. Ch. Postma, L. Balents, and C. Dekker, Nature (London) **402**, 273 (1999).
[47] H. Ishii, H. Kataura, H. Shiozawa, H. Yoshioka, H. Otsubo, Y. Takayama, T. Miyahara, S. Suzuki, Y. Achiba, M. Nakatake, T. Narimura, M. Higashiguchi, K. Shimada, H. Namatame, and M. Taniguchi, Nature (London) **426**, 540 (2003).
[48] R. Egger, Phys. Rev. Lett. **83**, 5547 (1999).
[49] K. Liu, Ph. Avouris, R. Martel, and W. K. Hsu, Phys. Rev. B **63**, 161404(R) (2001).
[50] A. Bachtold, M. de Jonge, K. Grove-Rasmussen, P. L. McEuen, M. Buitelaar, and C. Schönenberger, Phys. Rev. Lett. **87**, 166801 (2001).
[51] E. Graugnard, P. J. de Pablo, B. Walsh, A. W. Ghosh, S. Datta, and R. Reifenberger, Phys. Rev. B **64**, 125407 (2001).
[52] R. Tarkiainen, M. Ahlskog, J. Penttilä, L. Roschier, P. Hakonen, M. Paalanen, and E. Sonin, Phys. Rev. B **64**, 195412 (2001).
[53] A. Kanda, K. Tsukagoshi, Y. Aoyagi, and Y. Ootuka, Phys. Rev. Lett. **92**, 036801 (2004).
[54] J. Voit, Rep. Prog. Phys. **57**, 977 (1994).